Measurements of higher alkanes using NO+ chemical ionization in PTR-ToF-MS: important contributions of higher alkanes to secondary organic aerosols in China

Chaomin Wang[1,2], Bin Yuan [1,2,*], Caihong Wu[1,2], Sihang Wang[1,2], Jipeng Qi[1,2], Baolin Wang[3], Zelong Wang[1,2], Weiwei Hu[4], Wei Chen[4], Chenshuo Ye[5], Wenjie Wang[5], Yele Sun[6], Chen Wang[3], Shan Huang[1,2], Wei Song[4], Xinming Wang[4], Suxia Yang[1,2], Shenyang Zhang[1,2], Wanyun Xu[7], Nan Ma[1,2], Zhanyi Zhang[1,2], Bin Jiang[1,2], Hang Su[8], Yafang Cheng[8], Xuemei Wang[1,2], Min Shao[1,2,*]

[1] Institute for Environmental and Climate Research, Jinan University, 511443 Guangzhou, China

[2] Guangdong-Hongkong-Macau Joint Laboratory of Collaborative Innovation for Environmental Quality, 511443 Guangzhou, China

[3] School of Environmental Science and Engineering, Qilu University of Technology (Shandong Academy of Sciences), 250353 Jinan, China

[4] State Key Laboratory of Organic Geochemistry and Guangdong Key Laboratory of Environmental Protection and Resources Utilization, Guangzhou Institute of Geochemistry, Chinese Academy of Sciences, 510640 Guangzhou, China

[5] State Joint Key Laboratory of Environmental Simulation and Pollution Control, College of Environmental Sciences and Engineering, Peking University, 100871 Beijing, China

[6] State Key Laboratory of Atmospheric Boundary Physics and Atmospheric Chemistry, Institute of Atmospheric Physics, Chinese Academy of Sciences, 100029 Beijing, China

[7] State Key Laboratory of Severe Weather & Key Laboratory for Atmospheric Chemistry of China Meteorology Administration, Chinese Academy of Meteorological Sciences, 100081 Beijing, China

[8] Multiphase Chemistry Department, Max Planck Institute for Chemistry, Mainz 55128, Germany

*Email: Bin Yuan (byuan@jnu.edu.cn) and Min Shao (mshao@pku.edu.cn)

25 **Abstract:** Higher alkanes are a major class of intermediate-volatility organic compounds

26 (IVOCs), which have been proposed to be important precursors of secondary organic

27 aerosols (SOA) in the atmosphere. Accurate estimation of SOA from higher alkanes and

28 their oxidation processes in the atmosphere are limited, partially due to difficulty in their

29 measurements. High-time resolution (10 s) measurements of higher alkanes were performed

30 using NO^+ chemical ionization in proton transfer reaction time-of-flight mass spectrometer

31 (NO^+ PTR-ToF-MS) method at an urban site of Guangzhou in Pearl River Delta (PRD) and

32 at a rural site in North China Plain (NCP), respectively. High concentrations were observed

33 in both environments, with significant diurnal variations. At both sites, SOA production from

34 higher alkanes is estimated from their photochemical losses and SOA yields. Higher alkanes

35 account for significant fractions of SOA formation at the two sites, with average

36 contributions of 7.0±8.0% in Guangzhou and 9.4±9.1% in NCP, which are comparable or

37 even higher than both single-ring aromatics and naphthalenes. The significant contributions

38 of higher alkanes in SOA formation suggests that they should be explicitly included in

39 current models for SOA formation. Our work also highlights the importance of NO^+ PTR-

40 ToF-MS in measuring higher alkanes and quantifying their contributions to SOA formation.

1. Introduction

As important components of fine particles, secondary organic aerosols (SOA) not only affect air quality and climate change, but also threaten human health (An et al., 2019;Zhu et al., 2017;Chowdhury et al., 2018). Recent studies indicate large discrepancies between simulations and observations for SOA (de Gouw et al., 2008;Dzepina et al., 2009;Jiang et al., 2012), which are attributed to limited understanding of complicated chemical and physical processes underlying SOA formation (Hallquist et al., 2009). A volatility basis set (VBS) model was developed to advance SOA modeling by improving the modeling of further multigenerational oxidation processes and incorporating numerous, yet unidentified, low-volatility precursors of SOA (Donahue et al., 2006), which substantially improved the agreement between SOA simulations and observations (Hodzic et al., 2010). However, there are still large uncertainties in current VBS models, including rate constants of oxidation reactions, the change of O/C ratio in oxidation, and the relative importance of functionalization and fragmentation (Ma et al., 2017;Hayes et al., 2015). Explicit consideration of individual or a group of important semi-volatile or intermediate volatile organic compounds (S/I-VOCs) in the SOA model are urgently needed.

Higher alkanes as a major class of IVOCs (roughly corresponding to alkanes with 12-20 carbons) have been proposed as important SOA contributors in urban areas (Robinson et al., 2007;Yuan et al., 2013;Zhao et al., 2014a). In the typical urban areas, higher alkanes are reported to be mainly from vehicle emissions including diesel exhaust (Zhao et al., 2015) and gasoline exhaust (Zhao et al., 2016), corresponding generally to ~4% of nonmethane hydrocarbons (NMHCs) emissions from on-road vehicles. Higher alkanes are estimated to produce as much as or even more SOA than single-ring aromatics and polycyclic aromatic hydrocarbons from the oxidation of vehicle emissions, based on the chemical compositions

66   measurements of vehicle exhausts (Zhao et al., 2016, 2015). Based on vehicle exhaust tests,

67   higher alkanes were found to contribute ~37% to diesel exhaust-derived SOA and ~0.8% to

68   gasoline exhaust-derived SOA, respectively (Gentner et al., 2012). Previous model studies

69   suggested that SOA simulation can be significantly improved when higher alkanes were

70   considered in the model (Pye and Pouliot, 2012;Jathar et al., 2014;Wu et al., 2019). Although

71   the concentrations of higher alkanes might be lower than other VOCs classes (e.g. aromatics)

72   in the atmosphere, higher alkanes are found to have much higher SOA yields and the yields

73   increase steadily with carbon number (Lim and Ziemann, 2005;Lim and Ziemann,

74   2009;Presto et al., 2010b). For a given carbon number, SOA yields of higher alkanes reduce

75   with branching of the carbon chain, especially under high-NO_x conditions (Lim and Ziemann,

76   2009;Tkacik et al., 2012;Loza et al., 2014).

77   Higher alkanes have been mainly measured by gas chromatography-based techniques,

78   focusing on the compositions (Gong et al., 2011;Caumo et al., 2018), atmospheric

79   concentration levels (Bi et al., 2003;Anh et al., 2018) and gas-particle partitioning (Xie et al.,

80   2014;Sangiorgi et al., 2014). While most of previous studies collected offline samples

81   (usually 0.5 day-1 week) for GC-based analysis in the laboratory, hourly online

82   measurements of n-alkanes using GC-based thermal desorption aerosol gas chromatograph

83   for semi-volatile organic compounds (SV-TAG) was recently developed and applied in

84   ambient air (Zhao et al., 2013). Proton-transfer-reaction mass spectrometry (PTR-MS) using

85   H_3O^+ as reagent ions are capable of measurements for many organic compounds with high

86   time response and sensitivity (de Gouw and Warneke, 2007;Jordan et al., 2009;Yuan et al.,

87   2017b). Although H_3O^+ PTR-MS is responsive to large alkanes (>C8), these alkanes usually

88   fragment into small masses with mass spectra difficult to interpret (Jobson et al.,

89   2005;Gueneron et al., 2015). Recently, PTR-MS using NO^+ as reagent ions was

90   demonstrated to provide fast online measurement of higher alkanes (Koss et al.,

91   2016;Inomata et al., 2013). The high-time resolution measurements of higher alkanes

92   provide valuable information for SOA estimation, as the dependence of SOA yields on

93   organic aerosol concentrations and other environmental parameters (e.g. temperature) (Lim

94   and Ziemann, 2009;Presto et al., 2010b;Loza et al., 2014;Lamkaddam et al., 2017a) can be

95   taken into account in more detail.

96   In this study, we utilize NO^+ chemical ionization in PTR-ToF-MS (here referred as

97   NO^+ PTR-ToF-MS) to measure higher alkanes at two different sites in China, one urban site

98   in Pearl River Delta region and one rural site in North China Plain region. We use the datasets

99   along with measurements of other pollutants to estimate contributions to SOA formation

100   from higher alkanes and other SOA precursors. The observation-constrained SOA formation

101   of this study is a step forward upon previous modelling studies, which proposed the

102   important roles of S/I-VOCs (Jiang et al., 2012;Yang et al., 2018;Wu et al., 2019) including

103   higher alkanes (Yuan et al., 2013) in SOA formation in China.

2. Methods

105   Field campaigns were conducted at an urban site of Guangzhou in the Pearl River

106   Delta (PRD) region during September-November 2018 and at a rural site of Baoding in North

107   China Plain (NCP) during November-December 2018, respectively. The detailed description

108   of the measurement sites can be found in Supporting Information (SI, Figure S1).

2.1 NO^+ PTR-ToF-MS measurements

110   Proton-transfer-reaction mass spectrometry (PTR-MS) is a technique that allows for

111   fast and sensitive measurements of volatile organic compounds (VOCs) at trace levels in air.

112   PTR-MS using H_3O^+ chemistry has been demonstrated to measure alkenes, aromatics, and

113   even oxygenated VOCs (Yuan et al., 2017a;Wu et al., 2020). Here, PTR-MS with NO^+

114 chemistry was used to detect higher alkanes, through hydride abstraction by NO^+ forming

115 mass (m-1) ions (m is the molecular mass) (Koss et al., 2016;Inomata et al., 2013).

116   A commercially available PTR-ToF-MS instrument (Ionicon Analytik, Austria) with

117 a mass resolving power of 4000 m/Δm was used for this work. To generate NO^+ as reagent

118 ions, ultra-high-purity air (5.0 sccm) was directed into the hollow cathode discharge ion

119 source. The pressure of the drift tube was maintained at 3.8 mbar. Voltages of ion source and

120 drift chamber were explored (Figure S2) in the laboratory to optimize the generation of NO^+

121 ions relative to H_3O^+, O_2^+, and NO_2^+ and minimize alkane fragmentation. The intensities of

122 primary ion NO^+ and impurites (O_2^+, H_3O^+ and NO_2^+) and the ratio of O_2^+ to NO^+ during two

123 campaigns are shown in Figure S3 and Figure S4, respectively. The ratio of O_2^+/NO^+ (Figure

124 S4 (**a**)) is basically stable at 2-4% during the PRD campaign except during Oct. 26-Nov. 2,

125 2018 (7-10%). For the NCP campaign, the ratio of O_2^+/NO^+ (Figure S4 (**b**)) fluctuates between

126 10-40% in the early stage of campaign and keeps stable at ~20% in the later stage of the

127 campaign. Such fluctuations are atrributed to the humidity effect in the ambient air (Figure

128 S5). Ion source voltages of Us and Uso were selected as 40 V and 100 V, while Udrift and

129 Udx were set to 470 V and 23.5 V, resulting in an E/N (electric potential intensity relative to

130 gas number density of 60 Td. NO^+ PTR-ToF-MS data was analysed using Tofware software

131 (Tofwerk AG) for high-resolution peak-fitting. A description of the algorithm can be found

132 in Stark et al. (2015) and Timonen et al. (2016). Figure 1 shows the high-resolution peak

133 fitting to the averaged mass spectra on a typical day (12 October 2018) for m/z 169, m/z 211

134 and m/z 281, at which masses produced by dodecane ($C_{12}H_{25}^+$), pentadecane ($C_{15}H_{31}^+$) and

135 eicosane ($C_{20}H_{41}^+$) are detected. It is observed that the ions from higher alkanes lie at the right-

136 most position at each nominal mass, with signals either the largest or among the largest ions

137 at these nominal masses, which help to achieve high precision for determined signals of higher

138 alkanes from high-resolution peak fitting (Cubison and Jimenez, 2015;Corbin et al., 2015).

139   In this study, we normalize the raw ion count rate of higher alkanes to the primary ion

140   (NO^+) at a level of 10^6 cps to account for fluctuations of ion source and detector. Calibrations

141   were conducted every 1-2 days under both dry conditions (RH<1%) and ambient humidity

142   conditions using a gas standard with a series of n-alkanes (Apel Riemer Environmental Inc.)

143   during NCP campaign (Figure 2(a)). Sensitivities of n-alkanes (C8-C15) standards were

144   obtained during the campaign (Figure S6), which is defined as the normalized signal of hydride

145   abstraction ions for each higher alkane at 1 ppbv with a unit of ncps/ppb. The fluctuations of

146   sensitivities during the NCP campaign may be influenced by the variations of O_2^+ signals

147   (Figure 2), because the reactions of O_2^+ with alkanes can be proceeded by both charge transfer

148   and hydride abstraction (Amador et al., 2016) that may affect the ion signals of alkanes with

149   NO^+ reactions. Therefore, we use the daily ambient calibrations results to quantify the

150   concentration of higher alkanes during the NCP campaign to reflect the variations of sensitivity

151   from day to day. For the measurements without daily calibrations, we used closest calibration

152   results according to corresponding ambient O_2^+/NO^+ ratios and ambient humidity. Since we got

153   the alkanes standard at the very late period of the PRD campaign, we did not have the daily

154   calibrations for this campaign. Therefore, we use the sensitivity of each alkane under

155   corresponding O_2^+/NO^+ condition obtained from lab experiments after this campaign and also

156   consider the humidity effects (Figure 3(b, c)) to quantify the concentration of higher alkanes

157   during the PRD campaign. Humidity-dependent behaviours of n-alkanes (C8-C15) were

158   performed in the laboratory under different humidity (0-33 mmol/mol) by diluting higher

159   alkanes standard into humidified air to reach approximately 1 ppb mixing ratio. As shown in

160   Figure 3(b, c) and Figure S7 (a), the normalized signal of all product ions (m-1) and the

161   fragment ions of n-alkanes (C8-C15) standards are decreasing with the increase of humidity.

162   These decreasing patterns are probably due to the decreasing primary reagent ions (NO^+ and

163   O_2^+) as the humidity increases Figure S7(b). Thus, the humidity correction should be applied

164   for the quantitation of higher alkanes using NO^+ PTR-ToF-MS.

165   The fragmentation patterns for selected *n*-alkanes and their branched isomers are

166   measured with NO^+ PTR-ToF-MS by introducing commercially acquired pure chemicals

167   (Figure S8). Figure 4(a) shows the fractions of hydride abstraction m-1 ions in the mass

168   spectra of C8-C20 *n*-alkanes in NO^+ PTR-ToF-MS. Generally, larger *n*-alkanes show less

169   degree of fragmentation in the mass spectra with higher fractions contributed by m-1 ions.

170   The fractions of m-1 ions account for more than 60% of total ion signals for >C12 *n*-alkanes.

171   We also observe good correlation between the fractions of m-1 ions in mass spectra and the

172   determined sensitivities for C8-C15 *n*-alkanes. As C16-C21 *n*-alkanes exhibit similar degrees

173   of fragmentation as C15, sensitivities of the alkanes were assumed to be same as that of C15

174   *n*-alkane (Figure 4(b)). Comparison of the degree of fragmentation between *n*-alkanes and

175   their branched isomers (Figure S9) show the substituted groups affect little on the degrees of

176   fragmentations for product ions, at least for branched isomers with up to 4 substituted methyl

177   groups. Previous studies demonstrated that the branched alkanes from emissions of fossil fuel-

178   related sources are primarily with one or two alkyl branches (Chan et al., 2013;Isaacman et

179   al., 2012). Therefore, we conclude that the branched isomers of higher alkanes should have

180   similar response factors to their normal analogues. As a result, the concentration of higher

181   alkanes by NO^+ PTR-ToF-MS should be regarded as the summed concentrations of *n*-alkanes

182   and branched alkanes that have the same chemical formulas.

183   Detection limits are calculated as the concentrations at which signal counts are 3 times

184   of standard deviation of measured background counts (Bertram et al., 2011;Yuan et al., 2017b).

185   As shown in Table 1, detection limits are determined to be on the order of 0.7-1.3 ppt for

186   higher alkanes for 1 min integration times. Delay time is calculated as the time it takes for the

187   signal to drop to 10% of its initial value caused by the step-function change in sample

188   concentration (Pagonis et al., 2017). The delay times of higher alkanes for the field

189   measurements in this study and some other measurements (e.g. emission source

190   measurements and tubing losses test in the laboratory are summarized in Figure S10. It is

191   found that delay times for various alkanes are in a range of few seconds to few minutes, among

192   of which, higher-volatility alkanes (C8-C15) are better than 1 min and lower-volatility alkanes

193   (C16-C21) are relatively long reaching several minutes. These results suggest that alkanes

194   with higher carbon number, especially C20 and C21 might be influenced by the tubing delay

195   effect during the measurements. However, as shown later in section 3.1, the lower-volatility

196   alkanes exhibit very similar diurnal variations as higher-volotility alkanes during both

197   campaigns in PRD and NCP, implying that the tubing effects should not sinificantly affect on

198   temperoal variations of higher alkanes reported in this study.

199   During these two campaigns, PTR-ToF-MS automatically switches between H_3O^+ and

200   NO^+ chemistry every 10-20 minutes with a 10 s resolution of measurement. Switching

201   between H_3O^+ and NO^+ ion mode are provided by the PTR-MS Manager (v3.5) software

202   developed by the Ionicon Anlytik (Table S1). The pressures of drift chamber are held constant

203   at 3.8 mbar in both modes during the campaigns (Figure S11(a)). It usually takes <10 s for

204   H_3O^+ ions and ~60 s for NO^+ ions to re-stabilize after automatically switching between the

205   two measurement modes (Figure S11(b)). The ambient measurement data during the transition

206   period (~1 min) was discarded. Ambient air was continuously introduced into PTR-ToF-MS

207   through a Teflon tubing (1/4") with an external pump at 5.0 L/min, with tubing length of ~8

208   m and ~3 m during the PRD and the NCP campaign, respectively. The inlet tubing was heated

209   all the way to the sampling inlet to avoid water vapour condensation by an insulating tube

210   with a self-controlled heater wire (40 ℃) wrapping outside. The calculated residence time for

211   the inlet was ~3 s for PRD campaign and ~1 s for NCP campaign, respectively. The tubing

212   loss experiments were conducted in the laboratory by introducing standards of higher alkanes

213 (*n*-C8-C15), monoaromatics (benzene, toluene, o-xylene, 1,2,4-trimethylbenzene),

214 isoprenoids (isoprene, α-pinene) and naphthalene into PTR-ToF-MS through a 8 m Teflon

215 tubing (1/4") at room temperature with an external pump at 5.0 L/min (Figure S12). The

216 tubing loss of these compounds is found to be <5% except *n*-C15 (~8%) and naphthalene

217 (~10%). Background measurement of 3 minutes was conducted in each cycle of NO^+ and

218 H_3O^+ measurements by introducing the ambient air into a catalytic converter with a

219 temperature of 367 ℃.

2.2 Other measurements

221 During the Guangzhou campaign, an online GC-MS/FID system was used to measure

222 C2-C11 *n*-alkanes, alkenes and aromatics with a time resolution of one hour (Yuan et al.,

223 2012). Non-refractory components in particulate matter with diameter less than 1μm (PM_1)

224 including nitrate, sulfate, ammonium, chloride, and organics were measured with an

225 Aerodyne high-resolution time-of-flight aerosol mass spectrometric (HR-ToF-AMS) and a

226 time-of-flight aerosol chemical speciation monitor (ToF-ACSM) in PRD and NCP,

227 respectively. Trace gaseous species (CO, NO, NO_2, O_3, and SO_2) were measured using

228 commercial gas analyzers (Thermo Scientific). Photolysis frequencies were measured using

229 a spectroradiometer (PFS-100, Focused Photonics Inc.). In addition, temperature, pressure,

230 relative humidity and wind were continuously measured during two campaigns.

3. Results and Discussion

3.1 Ambient concentrations and diurnal variations of higher alkanes

233 Although NO^+ chemistry has been shown to be valuable in measuring many organic species,

234 the applications in real atmosphere of different environments are still rare (Koss et al., 2016).

235 Here, we compared the measurements of various VOCs from NO^+ PTR-ToF-MS with both

236   H_3O^+ PTR-ToF-MS and GC-MS/FID during the two campaigns. Overall, good agreements

237   between PTR-ToF-MS (both H_3O^+ and NO^+ chemistry) and GC-MS/FID are obtained for

238   aromatics and oxygenated VOCs except benzene (Figure S13, S14). Benzene measurements in

239   H_3O^+ chemistry show large difference with benzene measured from NO^+ chemistry in the

240   earlier period of PRD campaign (11 Sep.-14 Oct. 2018), but good agreement was obtained for

241   the rest of measurement period. Considering good agreement of benzene between NO^+ PTR-

242   ToF-MS and GC-MS/FID, we used benzene data from NO^+ measurement in this study. The

243   time series and diurnal variations of alkanes (C8-C11) between NO^+ PTR-ToF-MS and GC-

244   MS/FID are shown in Figure 5 (and Figure S15). Similar temporal trends for these alkanes are

245   observed from the two instruments. However, the diurnal patterns of total alkanes from NO^+

246   PTR-ToF-MS have a deeper afternoon trough than the *n*-alkanes measured by GC-MS,

247   implying that *n*-alkanes may have different temporal variations compared with those of total

248   alkanes. The concentrations at each carbon number from NO^+ PTR-ToF-MS are ~3-6 times

249   those from GC-MS/FID. This is expected, as dozens to hundreds of isomers exists for alkanes

250   with carbon number at this range (Goldstein and Galbally, 2007) and GC-MS/FID only

251   measured one or a few isomers. Based on measurements from NO^+ PTR-ToF-MS and GC-

252   MS/FID, we compute the molar concentration fractions of *n*-alkanes for each carbon number

253   (Figure 6 and Table S1). We found the fractions are in the range of 11%-21% for carbon

254   number of 8-11, which are comparable with results of ambient air in California, tunnel test and

255   vehicle exhausts (Figure 6 and Table S2) (Chan et al., 2013; Worton et al., 2014; Gentner et

256   al., 2012). These results indicate the importance of branched alkanes in concentrations of

257   higher alkanes and their potential contributions to SOA formation. It also has strong

258   implication for the merits of NO^+ PTR-ToF-MS in measuring sum of the alkanes with the same

259   formula for estimation of SOA contributions, as discussed later.

Table 2 summarizes means and standard deviations of concentrations of C8-C21 higher alkanes measured in PRD and in NCP, respectively. The mean concentrations of *n*-alkanes measured at a suburban site in Paris (Ait-Helal et al., 2014) and an urban site in Pasadena, U.S. are also included in Table 1 for comparison. According to the fraction of *n*-alkanes, the mean concentrations of *n*-alkanes in China are found to be comparable to that from Paris and higher than in Pasadena. In general, concentrations of higher alkanes concentration decrease with the increase of carbon number, with octanes (C8) at ~0.5 ppb and heneicosanes (C21) at ~0.002 ppb. This decreasing pattern of carbon distribution are as the results of lower emissions from sources (Gentner et al., 2012), larger reactivity towards OH radicals (Atkinson et al., 2008;Keyte et al., 2013) and larger fractions partitioning to particles (Liang et al., 1997;Xie et al., 2014;Zhao et al., 2013) in the atmosphere.

The diurnal variations of selected higher alkanes are shown in Figure 7. C12 alkanes and C15 alkanes exhibit similarly strong diurnal variations at both sites, with a relatively high levels at night and minimum concentrations detected in the late afternoon at both sites. Such diurnal patterns are consistent with other primary VOCs species (e.g. aromatics). In PRD, the diurnal variations of higher alkanes were as the result of faster chemical removal in the daytime and shallow boundary layer heights at night. Since OH concentrations in NCP during winter were much lower than that in PRD during autumn (Figure S16), diurnal variations of higher alkanes in NCP were mainly influenced by the change of boundary layer. The diurnal profiles of other higher alkanes are similar to C12 and C15 alkanes (Figure S17).

3.2 Estimation of the contributions of higher alkanes to SOA formation

A time-resolved approach based on consideration of photo-oxidation processes with OH radical (Ait-Helal et al., 2014) was applied to estimate contributions of higher alkanes to SOA during these two campaigns. In order to evaluate the relative importance to SOA

284   from different precursors, the same method was also used for monoaromatics, naphthalenes,

285   and isoprenoids.

286   This method considers the amount of chemical removal based on the parameterized

287   photochemical age, which was widely used to quantify contributions of different VOC

288   precursors to SOA formation (Zhao et al., 2014a;Ait-Helal et al., 2014;de Gouw et al., 2009).

289   The contributions to SOA formation from different compounds are determined by the ratios

290   of calculated SOA production amounts from individual precursors (SI, Appendix 2) and

291   SOA concentrations derived from factor analysis of OA measurements by AMS (SI,

292   Appendix 3). In this method, SOA formation for a given compound can be estimated by

293    $$[SOA_i]_t = [VOC_i]_t \times (e^{k_{VOC_i} \times ([OH] \times \Delta t)} - 1) \times Yield_i \qquad (1)$$

294   where $[SOA_i]_t$ is the calculated SOA production (μg m^{-3}) for a given specific compound VOC_i

295   at time t, $[VOC_i]_t$ is the VOC_i concentration measured at time t (μg m^{-3}), $Yield_i$ is the SOA

296   yield data summarized from chamber studies, k_{VOC_i} is the rate constant of VOC_i with the OH

297   radical (cm^3 molecule^{-1} s^{-1}). $[OH]$ is the OH concentration (molecules cm^{-3}), Δt is the

298   photochemical age. In this study, we calculate the $[OH] \times \Delta t$ (molecules cm^{-3} s), which was

299   considered as OH exposure in some studies (Jimenez et al., 2009). The OH exposure is

300   estimated by the ratio m+p-xylene and ethylbenzene with different reactivity for anthropogenic

301   VOCs and by the oxidation processes of isoprene for biogenic VOCs, respectively (Apel et al.,

302   2002;Roberts et al., 2006) (see details in SI, Appendix 4 and Figure S18). Since biogenic

303   emissions were pretty weak during cold winter (mean temperature 0.5±3.6 °C) during NCP

304   campaign, measured concentrations of isoprene and monoterpenes are attributed to be of

305   anthropogenic origin during the winter campaign in NCP campaign, especially given the fact

306   that they showed similar variations, diurnal profiles and strong correlation with CO and

307   anthropogenic VOCs species (Figure S19). A previous study in Helsinki also found the

308 importance of anthropogenic emission in monoterpene concentrations (Hellén et al., 2012).

309 Based on equation (1), SOA production from higher alkanes (C8-C21 alkanes),

310 monoaromatics (benzene, toluene, C8 aromatics, C9 aromatics, styrene), naphthalenes

311 (naphthalene, methylnaphthalenes, dimethylnaphthalenes) and isoprenoids (isoprene,

312 monoterpenes) were calculated. The concentration data of higher alkanes, isoprenoids and

313 benzene were taken from measurements of NO^+ PTR-ToF-MS. The concentration data of

314 naphthalenes (Figure S20) and monoaromatics except benzene were taken from

315 measurements of H_3O^+ PTR-ToF-MS. The detail about the H_3O^+ PTR-ToF-MS measurements

316 can be found in Wu et al. (2020). The OH reaction rate constant of each compound was taken

317 from literature (Atkinson, 2003). SOA yield data used here for higher alkanes (Lim and

318 Ziemann, 2009;Presto et al., 2010a;Loza et al., 2014;Lamkaddam et al., 2017b),

319 monoaromatics (Li et al., 2016;Ng et al., 2007;Tajuelo et al., 2019), naphthalenes (Chan et al.,

320 2009) and isoprenoids (Ahlberg et al., 2017;Carlton et al., 2009;Edney et al., 2005;Kleindienst

321 et al., 2006;Pandis et al., 1991) were summarized from reported values in the literature, with

322 the consideration of the influence of organic aerosol concentration (Figure S21) to SOA yields

323 (Donahue et al., 2006) (Figure S22-23). SOA yields under high NO_x conditions are used in

324 this study, as relatively high NO_x concentrations in PRD (42.6±33.7 ppb) and in NCP

325 (81.7±57.0 ppb) (Figure S24) would cause RO_2 radicals from organic compounds mainly

326 reacting with NO (Bahreini et al., 2009).

327 Both OH reaction rate constants and SOA yields of *n*-alkanes reported in the literature

328 are applied for higher alkanes, as most of the chamber studies have focused on n-alkanes.

329 Considering the SOA yields of branched alkanes are lower than *n*-alkanes, which is depending

330 on chemical structures of the carbon backbone (Lim and Ziemann, 2009;Tkacik et al.,

331 2012;Loza et al., 2014), the estimation of SOA from alkanes in this study might be a little

332 overestimated. As shown above, temperature (mean temperature 0.5±3.6 °C) in NCP winter

333 campaign was significantly lower than the temperature (usually 25 °C) at which SOA yields

334 are derived from chamber studies. Temperature can significantly influence SOA yields, with

335 higher yields at lower temperature (Takekawa et al., 2003;Lamkaddam et al., 2017b). It might

336 cause underestimation of SOA production from various precursors in winter of NCP.

337 The calculated results of SOA production for different higher alkanes are shown in

338 Figure 8. Although lower concentrations of heavier alkanes were observed for both

339 campaigns, the calculated SOA production are largest for C12-C18 (Figure 8(b)). This is

340 because of two reasons: (1) Alkanes with larger carbon number have larger SOA yields. The

341 calculated average SOA yields (Table S3) during the two campaigns are both larger than 0.2

342 for >C12 alkanes and increase to near unity for C20-C21 alkanes. (2) Larger alkanes are

343 relatively more reactive than lighter ones, which results in larger proportions of calculated

344 concentrations that have been chemically consumed in the atmosphere (the concentrations

345 labelled "consumed" in Figure 8(a)). The distribution of contributions from alkanes with

346 different carbon number to SOA formation shown here is in good agreement with the

347 previous results referred from volatility calculation for precursors (de Gouw et al.,

348 2011;Liggio et al., 2016). The peaks in alkanes SOA productions occur around C15 in both

349 campaigns of PRD and NCP, which is a great result that shows the importance of IVOCs on

350 SOA.

351 Along with higher alkanes, SOA production for monoaromatics, naphthalenes and

352 isoprenoids are shown in Figure 9 (and Figure S25-27). Compared to monoaromatics, higher

353 alkanes are associated with lower concentrations (Figure S28). However, higher alkanes play

354 an important role in SOA formation due to their high SOA yields (Figure S29). The total

355 average SOA production from C8-C21 alkanes are 0.6±0.8 μg m^{-3} and 0.7±0.8 μg m^{-3} in PRD

356 and NCP, respectively. The formed SOA from higher alkanes account for 7.0±8.0% and

357 9.4±9.1% of SOA formation in PRD and NCP, respectively. The contributions of

358 monoaromatics to SOA formation are 6.2±7.7% and 9.4±17.4% in PRD and NCP,

359 respectively. Naphthalenes have been proposed to be important precursors of SOA from

360 laboratory chamber studies (Kleindienst et al., 2012). In this study, we determine 2.8±4.6%

361 of SOA in PRD and 11.1±14.3% of SOA in NCP are contributed by naphthalenes. The SOA

362 contribution from naphthalenes determined for NCP is comparable to the results (10.2±1.0%)

363 obtained during haze events in Beijing in a recent study (Huang et al., 2019). Significant

364 contribution from monoterpenes to SOA (8.7±14.6%) is observed in NCP. As mentioned

365 above, we attribute these isoprene and monoterpenes to anthropogenic emissions in this region.

366 The SOA precursors considered in this study in total could explain 14.9%-29.0% and 16.4-

367 125.3% of SOA formation in PRD and NCP, respectively. The influence of chamber-based

368 vapour wall losses on SOA yields was examined in previous studies (Zhang et al., 2014) and

369 the results show that the literature reported SOA yields are low by factors of ~1.1-2.2 for the

370 high NO_x conditions (Table S4). This suggests that the SOA estimations in this study might

371 be correspondingly underestimated. The low explained percentages of SOA formations in

372 both of PRD and NCP (Figure 9(c, d)) imply that some other SOA precursors (e.g.

373 alkylcyclohexanes, alkylbenzenes, cyclic and polycyclic aliphatic materials) (Zhao et al.,

374 2015; Drozd et al., 2019) or formation pathways (e.g. aqueous reactions) (Kuang et al., 2020)

375 are contributing significantly to SOA formation. Compared to a previous study in northern

376 China (Yuan et al., 2013), the missing gap of SOA formation declined after explicitly

377 considering higher alkanes and naphthalenes in SOA production.

378 As shown in Figure 9, we find that C8-C21 higher alkanes contribute significantly to

379 SOA formation at both an urban site in autumn of PRD and a rural site in winter of NCP.

380 The contributions from higher alkanes are either comparable or higher than both

381 monoaromatics and naphthalenes. Another estimation method by considering SOA

382 instantaneous production rates obtained similar results (Figure S30), which confirms the

383   results from the photochemical age based on parameterization method shown above. The

384   importance of higher alkanes in SOA formation has been also proposed in several previous

385   SOA modelling studies (Pye and Pouliot, 2012;Zhao et al., 2014b). These results, along with

386   our results from observations in ambient atmosphere, underline that the inclusion of higher

387   alkanes in SOA models in the atmosphere should be considered if possible.

4. Concluding remarks

389   In this study, we utilized a NO^+ PTR-ToF-MS to measure C8-C21 alkanes in two different

390   environments in China. Based on a series of laboratory experiments, we show that NO^+ PTR-

391   ToF-MS can provide online measurements of higher alkanes with high accuracy and fast

392   response. The measured concentrations of higher alkanes were relatively high during the two

393   campaigns. The diurnal profiles of higher alkanes are similar to anthropogenic VOCs,

394   implying they are emitted from anthropogenic sources.

395   On the basis of measurements of higher alkanes by NO^+ PTR-ToF-MS, we successfully

396   take into account their contributions in SOA formation. The time-resolved measurements of

397   higher alkanes by NO^+ PTR-ToF-MS provide the opportunity to accurately apply the

398   photochemical age-based parameterization method. As there is no separation before detection

399   in PTR-ToF-MS, the measured concentrations of NO^+ PTR-ToF-MS represent all of the

400   compounds that contribute to the product ions (m-1 ions), which include concentrations from

401   both *n*-alkanes and branched alkanes. With the total concentration of both *n*-alkanes and

402   branched alkanes quantified, the contribution from higher alkanes at each carbon number can

403   be estimated as a whole. This is an important supplementary method to the traditional

404   analytical method by GC techniques for higher alkanes, as fully chemical separation and

405   detection of numerous isomers of higher alkanes remain as a challenge, even using the most

406   advanced GC×GC-ToF-MS instruments (Chan et al., 2013;Alam et al., 2016).

407    Higher alkanes were found to have significant contributions to SOA in both PRD and

408 NCP regions with a similar or even higher contributions than that of monoaromatics and

409 naphthalenes. The importance of higher alkanes to SOA formation also call for more work

410 to investigate emissions and chemistry of these compounds in the atmosphere. It was shown

411 that fossil-related combustions such as vehicle exhausts are major sources for higher alkanes

412 (Zhao et al., 2016). While, recent studies have shown that non-combustion sources, such as

413 the use of solvents, have a potentially significant impact on high-alkane emissions

414 (McDonald et al., 2018;Khare and Gentner, 2018). However, such quantitative information

415 on emissions of higher alkanes is still limited. The measurements of higher alkanes by NO^+

416 PTR-ToF-MS with fast response could help to fill these research gaps.

417

Acknowledgements

This work was supported by the National Key R&D Plan of China (grant No. 2018YFC0213904, 2016YFC0202206), the National Natural Science Foundation of China (grant No. 41877302 and No. 91644215), Guangdong Natural Science Funds for Distinguished Young Scholar (grant No. 2018B030306037), Guangdong Provincial Key R&D Plan (grant No. 2019B110206001), Guangdong Soft Science Research Program (grant No. 2019B101001005) and Guangdong Innovative and Entrepreneurial Research Team Program (grant No. 2016ZT06N263). Weiwei Hu and Wei Chen were supported by National Natural Science Foundation of China (grant No. 41875156). The authors gratefully acknowledge the science team for their technical support and discussions during the campaigns in PRD and NCP.

Data availability

Data is available from the authors upon request

Competing interests

The authors declare that they have no conflicts of interest

Author contributions

BY and MS designed the research. CMW, CHW, SHW, JPQ, BLW, WC, CW, WS and WYX contributed to data collection. CMW performed the data analysis, with contributions from ZLW, WWH, SXY and CSY. CMW and BY prepared the manuscript with contributions from other authors. All the authors reviewed the manuscript.

References

438

439 Ahlberg, E., Falk, J., Eriksson, A., Holst, T., Brune, W. H., Kristensson, A., Roldin, P., and

440 Svenningsson, B.: Secondary organic aerosol from VOC mixtures in an oxidation flow reactor,

441 Atmospheric Environment, 161, 210-220, 10.1016/j.atmosenv.2017.05.005, 2017.

442 Ait-Helal, W., Borbon, A., Sauvage, S., de Gouw, J. A., Colomb, A., Gros, V., Freutel, F., Crippa, M.,

443 Afif, C., Baltensperger, U., Beekmann, M., Doussin, J. F., Durand-Jolibois, R., Fronval, I., Grand, N.,

444 Leonardis, T., Lopez, M., Michoud, V., Miet, K., Perrier, S., Prevot, A. S. H., Schneider, J., Siour, G.,

445 Zapf, P., and Locoge, N.: Volatile and intermediate volatility organic compounds in suburban Paris:

446 variability, origin and importance for SOA formation, Atmospheric Chemistry and Physics, 14, 10439-

447 10464, 10.5194/acp-14-10439-2014, 2014.

448 Alam, M. S., Stark, C., and Harrison, R. M.: Using Variable Ionization Energy Time-of-Flight Mass

449 Spectrometry with Comprehensive GCxGC To Identify Isomeric Species, Analytical Chemistry, 88,

450 4211-4220, 10.1021/acs.analchem.5b03122, 2016.

451 Amador, O., Misztal, P., Weber, R., Worton, D., Zhang, H., Drozd, G., and Goldstein, A.: Sensitive

452 detection of n -alkanes using a mixed ionization mode proton-transfer-reaction mass spectrometer,

453 Atmospheric Measurement Techniques, 9, 5315-5329, 10.5194/amt-9-5315-2016, 2016.

454 An, Z., Huang, R. J., Zhang, R., Tie, X., Li, G., Cao, J., Zhou, W., Shi, Z., Han, Y., Gu, Z., and Ji, Y.:

455 Severe haze in northern China: A synergy of anthropogenic emissions and atmospheric processes, Proc

456 Natl Acad Sci U S A, 116, 8657-8666, 10.1073/pnas.1900125116, 2019.

457 Anh, H. Q., Tomioka, K., Tue, N. M., Tuyen, L. H., Chi, N. K., Minh, T. B., Viet, P. H., and Takahashi,

458 S.: A preliminary investigation of 942 organic micro-pollutants in the atmosphere in waste processing

459 and urban areas, northern Vietnam: Levels, potential sources, and risk assessment, Ecotoxicol. Environ.

460 Saf., 167, 354-364, 2018.

461 Apel, E. C., Riemer, D. D., Hills, A., Baugh, W., Orlando, J., Faloona, I., Tan, D., Brune, W., Lamb,

462 B., Westberg, H., Carroll, M. A., Thornberry, T., and Geron, C. D.: Measurement and interpretation of

463 isoprene fluxes and isoprene, methacrolein, and methyl vinyl ketone mixing ratios at the PROPHET

464 site during the 1998 Intensive, Journal of Geophysical Research: Atmospheres, 107, ACH 7-1-ACH 7-

465 15, 10.1029/2000JD000225, 2002.

466 Atkinson, R.: Kinetics of the gas-phase reactions of OH radicals with alkanes and cycloalkanes,

467 Atmospheric Chemistry and Physics, 3, 2233-2307, 10.5194/acp-3-2233-2003, 2003.

468 Atkinson, R., Arey, J., and Aschmann, S. M.: Atmospheric chemistry of alkanes: Review and recent

469 developments, Atmospheric Environment, 42, 5859-5871, 10.1016/j.atmosenv.2007.08.040, 2008.

470 Bertram, T., Kimmel, J., Crisp, T., Ryder, O., Yatavelli, R., Thornton, J., Cubison, M., Gonin, M., and

471 Worsnop, D.: A field-deployable, chemical ionization time-of-flight mass spectrometer, Atmospheric

472 Measurement Techniques, 4, 1471-1479, 10.5194/amt-4-1471-2011, 2011.

473 Bi, X. H., Sheng, G. Y., Peng, P., Chen, Y. J., Zhang, Z. Q., and Fu, J. M.: Distribution of particulate-

474 and vapor-phase n-alkanes and polycyclic aromatic hydrocarbons in urban atmosphere of Guangzhou,

475 China, Atmospheric Environment, 37, 289-298, 10.1016/s1352-2310(02)00832-4, 2003.

476 Carlton, A. G., Wiedinmyer, C., and Kroll, J. H.: A review of Secondary Organic Aerosol (SOA)

477 formation from isoprene, Atmospheric Chemistry and Physics, 9, 4987-5005, DOI 10.5194/acp-9-4987-

478 2009, 2009.

479 Caumo, S., Vicente, A., Custodio, D., Alves, C., and Vasconcellos, P.: Organic compounds in

480 particulate and gaseous phase collected in the neighbourhood of an industrial complex in Sao Paulo

481 (Brazil), Air Quality Atmosphere and Health, 11, 271-283, 10.1007/s11869-017-0531-7, 2018.

482 Chan, A. W. H., Kautzman, K. E., Chhabra, P. S., Surratt, J. D., Chan, M. N., Crounse, J. D., Kuerten,

483 A., Wennberg, P. O., Flagan, R. C., and Seinfeld, J. H.: Secondary organic aerosol formation from

484 photooxidation of naphthalene and alkylnaphthalenes: implications for oxidation of intermediate

485 volatility organic compounds (IVOCs), Atmospheric Chemistry and Physics, 9, 3049-3060,

486 10.5194/acp-9-3049-2009, 2009.

487 Chan, A. W. H., Isaacman, G., Wilson, K. R., Worton, D. R., Ruehl, C. R., Nah, T., Gentner, D. R.,

488 Dallmann, T. R., Kirchstetter, T. W., Harley, R. A., Gilman, J. B., Kuster, W. C., deGouw, J. A.,

489 Offenberg, J. H., Kleindienst, T. E., Lin, Y. H., Rubitschun, C. L., Surratt, J. D., Hayes, P. L., Jimenez,

490 J. L., and Goldstein, A. H.: Detailed chemical characterization of unresolved complex mixtures in

491 atmospheric organics: Insights into emission sources, atmospheric processing, and secondary organic

492   aerosol formation, Journal of Geophysical Research-Atmospheres, 118, 6783-6796,

493   10.1002/jgrd.50533, 2013.

494   Chowdhury, P. H., He, Q., Male, T. L., Brune, W. H., Rudich, Y., and Pardo, M.: Exposure of Lung

495   Epithelial Cells to Photochemically Aged Secondary Organic Aerosol Shows Increased Toxic Effects,

496   Environmental Science & Technology Letters, 5, 424-430, 10.1021/ars.estlett.8b00256, 2018.

497   Corbin, J. C., Othman, A., D. Allan, J., R. Worsnop, D., D. Haskins, J., Sierau, B., Lohmann, U., and

498   A. Mensah, A.: Peak-fitting and integration imprecision in the Aerodyne aerosol mass spectrometer:

499   effects of mass accuracy on location-constrained fits, Atmos. Meas. Tech., 8, 4615-4636, 10.5194/amt-

500   8-4615-2015, 2015.

501   Cubison, M. J., and Jimenez, J. L.: Statistical precision of the intensities retrieved from constrained

502   fitting of overlapping peaks in high-resolution mass spectra, Atmos. Meas. Tech., 8, 2333-2345,

503   10.5194/amt-8-2333-2015, 2015.

504   de Gouw, J., and Warneke, C.: Measurements of volatile organic compounds in the earths atmosphere

505   using proton-transfer-reaction mass spectrometry, Mass Spectrometry Reviews, 26, 223-257,

506   10.1002/mas.20119, 2007.

507   de Gouw, J. A., Brock, C. A., Atlas, E. L., Bates, T. S., Fehsenfeld, F. C., Goldan, P. D., Holloway, J.

508   S., Kuster, W. C., Lerner, B. M., Matthew, B. M., Middlebrook, A. M., Onasch, T. B., Peltier, R. E.,

509   Quinn, P. K., Senff, C. J., Stohl, A., Sullivan, A. P., Trainer, M., Warneke, C., Weber, R. J., and

510   Williams, E. J.: Sources of particulate matter in the northeastern United States in summer: 1. Direct

511   emissions and secondary formation of organic matter in urban plumes, Journal of Geophysical

512   Research-Atmospheres, 113, 10.1029/2007jd009243, 2008.

513   de Gouw, J. A., Welsh-Bon, D., Warneke, C., Kuster, W. C., Alexander, L., Baker, A. K., Beyersdorf,

514   A. J., Blake, D. R., Canagaratna, M., Celada, A. T., Huey, L. G., Junkermann, W., Onasch, T. B.,

515   Salcido, A., Sjostedt, S. J., Sullivan, A. P., Tanner, D. J., Vargas, O., Weber, R. J., Worsnop, D. R., Yu,

516   X. Y., and Zaveri, R.: Emission and chemistry of organic carbon in the gas and aerosol phase at a sub-

517   urban site near Mexico City in March 2006 during the MILAGRO study, Atmospheric Chemistry and

518   Physics, 9, 3425-3442, 10.5194/acp-9-3425-2009, 2009.

519 de Gouw, J. A., Middlebrook, A. M., Warneke, C., Ahmadov, R., Atlas, E. L., Bahreini, R., Blake, D.

520 R., Brock, C. A., Brioude, J., Fahey, D. W., Fehsenfeld, F. C., Holloway, J. S., Le Henaff, M., Lueb, R.

521 A., McKeen, S. A., Meagher, J. F., Murphy, D. M., Paris, C., Parrish, D. D., Perring, A. E., Pollack, I.

522 B., Ravishankara, A. R., Robinson, A. L., Ryerson, T. B., Schwarz, J. P., Spackman, J. R., Srinivasan,

523 A., and Watts, L. A.: Organic aerosol formation downwind from the Deepwater Horizon oil spill,

524 Science, 331, 1295-1299, 10.1126/science.1200320, 2011.

525 Donahue, N. M., Robinson, A. L., Stanier, C. O., and Pandis, S. N.: Coupled partitioning, dilution, and

526 chemical aging of semivolatile organics, Environmental Science & Technology, 40, 2635-2643,

527 10.1021/es052297c, 2006.

528 Drozd, G. T., Zhao, Y., Saliba, G., Frodin, B., Maddox, C., Oliver Chang, M. C., Maldonado, H., Sardar,

529 S., Weber, R. J., Robinson, A. L., and Goldstein, A. H.: Detailed Speciation of Intermediate Volatility

530 and Semivolatile Organic Compound Emissions from Gasoline Vehicles: Effects of Cold-Starts and

531 Implications for Secondary Organic Aerosol Formation, Environ. Sci. Technol., 53, 1706-1714,

532 https://doi.org/10.1021/acs.est.8b05600, 2019.

533 Dzepina, K., Volkamer, R. M., Madronich, S., Tulet, P., Ulbrich, I. M., Zhang, Q., Cappa, C. D.,

534 Ziemann, P. J., and Jimenez, J. L.: Evaluation of recently-proposed secondary organic aerosol models

535 for a case study in Mexico City, Atmospheric Chemistry and Physics, 9, 5681-5709, 10.5194/acp-9-

536 5681-2009, 2009.

537 Edney, E. O., Kleindienst, T. E., Jaoui, M., Lewandowski, M., Offenberg, J. H., Wang, W., and Claeys,

538 M.: Formation of 2-methyl tetrols and 2-methylglyceric acid in secondary organic aerosol from

539 laboratory irradiated isoprene/NOX/SO2/air mixtures and their detection in ambient PM2.5 samples

540 collected in the eastern United States, Atmospheric Environment, 39, 5281-5289,

541 https://doi.org/10.1016/j.atmosenv.2005.05.031, 2005.

542 Gentner, D. R., Isaacman, G., Worton, D. R., Chan, A. W. H., Dallmann, T. R., Davis, L., Liu, S., Day,

543 D. A., Russell, L. M., Wilson, K. R., Weber, R., Guha, A., Harley, R. A., and Goldstein, A. H.:

544 Elucidating secondary organic aerosol from diesel and gasoline vehicles through detailed

545 characterization of organic carbon emissions, Proceedings of the National Academy of Sciences of the

546 United States of America, 109, 18318-18323, 10.1073/pnas.1212272109, 2012.

547 Goldstein, A. H., and Galbally, I. E.: Known and Unexplored Organic Constituents in the Earth's

548 Atmosphere, Environmental Science & Technology, 41, 1514-1521, 10.1021/es072476p, 2007.

549 Gong, P., Wang, X., and Yao, T.: Ambient distribution of particulate- and gas-phase n-alkanes and

550 polycyclic aromatic hydrocarbons in the Tibetan Plateau, Environmental Earth Sciences, 64, 1703-1711,

551 10.1007/s12665-011-0974-3, 2011.

552 Gueneron, M., Erickson, M. H., VanderSchelden, G. S., and Jobson, B. T.: PTR-MS fragmentation

553 patterns of gasoline hydrocarbons, International Journal of Mass Spectrometry, 379, 97-109,

554 10.1016/j.ijms.2015.01.001, 2015.

555 Hallquist, M., Wenger, J. C., Baltensperger, U., Rudich, Y., Simpson, D., Claeys, M., Dommen, J.,

556 Donahue, N. M., George, C., Goldstein, A. H., Hamilton, J. F., Herrmann, H., Hoffmann, T., Iinuma,

557 Y., Jang, M., Jenkin, M. E., Jimenez, J. L., Kiendler-Scharr, A., Maenhaut, W., McFiggans, G., Mentel,

558 T. F., Monod, A., Prevot, A. S. H., Seinfeld, J. H., Surratt, J. D., Szmigielski, R., and Wildt, J.: The

559 formation, properties and impact of secondary organic aerosol: current and emerging issues,

560 Atmospheric Chemistry and Physics, 9, 5155-5236, 10.5194/acp-9-5155-2009, 2009.

561 Hayes, P. L., Carlton, A. G., Baker, K. R., Ahmadov, R., Washenfelder, R. A., Alvarez, S.,

562 Rappenglueck, B., Gilman, J. B., Kuster, W. C., de Gouw, J. A., Zotter, P., Prevot, A. S. H., Szidat, S.,

563 Kleindienst, T. E., Offenberg, J. H., Ma, P. K., and Jimenez, J. L.: Modeling the formation and aging

564 of secondary organic aerosols in Los Angeles during CalNex 2010, Atmospheric Chemistry and Physics,

565 15, 5773-5801, 10.5194/acp-15-5773-2015, 2015.

566 Hellén, H., Tykkä, T., and Hakola, H.: Importance of monoterpenes and isoprene in urban air in northern

567 Europe, Atmospheric Environment, 59, 59-66, https://doi.org/10.1016/j.atmosenv.2012.04.049, 2012.

568 Hodzic, A., Jimenez, J. L., Madronich, S., Canagaratna, M. R., DeCarlo, P. F., Kleinman, L., and Fast,

569 J.: Modeling organic aerosols in a megacity: potential contribution of semi-volatile and intermediate

570 volatility primary organic compounds to secondary organic aerosol formation, Atmospheric Chemistry

571 and Physics, 10, 5491-5514, 10.5194/acp-10-5491-2010, 2010.

572 Huang, G., Liu, Y., Shao, M., Li, Y., Chen, Q., Zheng, Y., Wu, Z., Liu, Y., Wu, Y., Hu, M., Li, X., Lu,

573 S., Wang, C., Liu, J., Zheng, M., and Zhu, T.: Potentially Important Contribution of Gas-Phase

574 Oxidation of Naphthalene and Methylnaphthalene to Secondary Organic Aerosol during Haze Events

575 in Beijing, Environmental Science & Technology, 53, 1235-1244, 10.1021/acs.est.8b04523, 2019.

576 Inomata, S., Tanimoto, H., and Yamada, H.: Mass Spectrometric Detection of Alkanes Using NO+

577 Chemical Ionization in Proton-transfer-reaction Plus Switchable Reagent Ion Mass Spectrometry,

578 Chemistry Letters, 43, 538-540, 10.1246/cl.131105, 2013.

579 Isaacman, G., Wilson, K. R., Chan, A. W. H., Worton, D. R., Kimmel, J. R., Nah, T., Hohaus, T., Gonin,

580 M., Kroll, J. H., Worsnop, D. R., and Goldstein, A. H.: Improved Resolution of Hydrocarbon Structures

581 and Constitutional Isomers in Complex Mixtures Using Gas Chromatography-Vacuum Ultraviolet-

582 Mass Spectrometry, Analytical Chemistry, 84, 2335-2342, 10.1021/ac2030464, 2012.

583 Jathar, S. H., Gordon, T. D., Hennigan, C. J., Pye, H. O. T., Pouliot, G., Adams, P. J., Donahue, N. M.,

584 and Robinson, A. L.: Unspeciated organic emissions from combustion sources and their influence on

585 the secondary organic aerosol budget in the United States, Proceedings of the National Academy of

586 Sciences of the United States of America, 111, 10473-10478, 10.1073/pnas.1323740111, 2014.

587 Jiang, F., Liu, Q., Huang, X., Wang, T., Zhuang, B., and Xie, M.: Regional modeling of secondary

588 organic aerosol over China using WRF/Chem, Journal of Aerosol Science, 43, 57-73,

589 10.1016/j.jaerosci.2011.09.003, 2012.

590 Jimenez, J. L., Canagaratna, M. R., Donahue, N. M., Prevot, A. S. H., Zhang, Q., Kroll, J. H. et al.

591 Evolution of Organic Aerosols in the Atmosphere, Science, 326(5959), 1525-1529,

592 10.1126/science.1180353, 2009.

593 Jobson, B. T., Alexander, M. L., Maupin, G. D., and Muntean, G. G.: On-line analysis of organic

594 compounds in diesel exhaust using a proton transfer reaction mass spectrometer (PTR-MS),

595 International Journal of Mass Spectrometry, 245, 78-89, 10.1016/j.ijms.2005.05.009, 2005.

596 Jordan, A., Haidacher, S., Hanel, G., Hartungen, E., Herbig, J., Maerk, L., Schottkowsky, R., Seehauser,

597 H., Sulzer, P., and Maerk, T. D.: An online ultra-high sensitivity Proton-transfer-reaction mass-

598 spectrometer combined with switchable reagent ion capability (PTR+SRI-MS), International Journal of

599 Mass Spectrometry, 286, 32-38, 10.1016/j.ijms.2009.06.006, 2009.

Keyte, I. J., Harrison, R. M., and Lammel, G.: Chemical reactivity and long-range transport potential of polycyclic aromatic hydrocarbons - a review, Chemical Society Reviews, 42, 9333-9391, 10.1039/c3cs60147a, 2013.

Khare, P., and Gentner, D. R.: Considering the future of anthropogenic gas-phase organic compound emissions and the increasing influence of non-combustion sources on urban air quality, Atmospheric Chemistry and Physics, 18, 5391-5413, 10.5194/acp-18-5391-2018, 2018.

Kleindienst, T. E., Edney, E. O., Lewandowski, M., Offenberg, J. H., and Jaoui, M.: Secondary Organic Carbon and Aerosol Yields from the Irradiations of Isoprene and α-Pinene in the Presence of NOx and SO2, Environmental Science & Technology, 40, 3807-3812, 10.1021/es052446r, 2006.

Kleindienst, T. E., Jaoui, M., Lewandowski, M., Offenberg, J. H., and Docherty, K. S.: The formation of SOA and chemical tracer compounds from the photooxidation of naphthalene and its methyl analogs in the presence and absence of nitrogen oxides, Atmospheric Chemistry and Physics, 12, 8711-8726, 10.5194/acp-12-8711-2012, 2012.

Koss, A. R., Warneke, C., Yuan, B., Coggon, M. M., Veres, P. R., and de Gouw, J. A.: Evaluation of NO+ reagent ion chemistry for online measurements of atmospheric volatile organic compounds, Atmospheric Measurement Techniques, 9, 2909-2925, 10.5194/amt-9-2909-2016, 2016.

Kuang, Y., He, Y., Xu, W., Yuan, B., Zhang, G., Ma, Z., Wu, C., Wang, C., Wang, S., Zhang, S., Tao, J., Ma, N., Su, H., Cheng, Y., Shao, M., and Sun, Y.: Photochemical Aqueous-Phase Reactions Induce Rapid Daytime Formation of Oxygenated Organic Aerosol on the North China Plain, Environmental Science & Technology, 10.1021/acs.est.9b06836, 2020.

Lamkaddam, H., Gratien, A., Pangui, E., Cazaunau, M., Picquet-Varrault, B., and Doussin, J.-F.: High-NOx Photooxidation of n-Dodecane: Temperature Dependence of SOA Formation, Environmental Science & Technology, 51, 192-201, 10.1021/acs.est.6b03821, 2017a.

Lamkaddam, H., Gratien, A., Pangui, E., Cazaunau, M., Picquet-Varrault, B., and Doussin, J. F.: High-NOx Photooxidation of n-Dodecane: Temperature Dependence of SOA Formation, Environ Sci Technol, 51, 192-201, 10.1021/acs.est.6b03821, 2017b.

626 Li, L., Tang, P., Nakao, S., Kacarab, M., and Cocker, D. R., 3rd: Novel Approach for Evaluating

627 Secondary Organic Aerosol from Aromatic Hydrocarbons: Unified Method for Predicting Aerosol

628 Composition and Formation, Environ Sci Technol, 50, 6249-6256, 10.1021/acs.est.5b05778, 2016.

629 Liang, C., Pankow, J. F., Odum, J. R., and Seinfeld, J. H.: Gas/Particle Partitioning of Semivolatile

630 Organic Compounds To Model Inorganic, Organic, and Ambient Smog Aerosols, Environmental

631 Science & Technology, 31, 3086-3092, 10.1021/es9702529, 1997.

632 Liggio, J., Li, S.-M., Hayden, K., Taha, Y. M., Stroud, C., Darlington, A., Drollette, B. D., Gordon, M.,

633 Lee, P., Liu, P., Leithead, A., Moussa, S. G., Wang, D., O'Brien, J., Mittermeier, R. L., Brook, J. R.,

634 Lu, G., Staebler, R. M., Han, Y., Tokarek, T. W., Osthoff, H. D., Makar, P. A., Zhang, J., L. Plata, D.,

635 and Gentner, D. R.: Oil sands operations as a large source of secondary organic aerosols, Nature, 534,

636 91-94, 10.1038/nature17646, 2016.

637 Lim, Y. B., and Ziemann, P. J.: Products and mechanism of secondary organic aerosol formation from

638 reactions of n-alkanes with OH radicals in the presence of NOx, Environmental Science & Technology,

639 39, 9229-9236, 10.1021/es051447g, 2005.

640 Lim, Y. B., and Ziemann, P. J.: Effects of Molecular Structure on Aerosol Yields from OH Radical-

641 Initiated Reactions of Linear, Branched, and Cyclic Alkanes in the Presence of NOx, Environmental

642 Science & Technology, 43, 2328-2334, 10.1021/es803389s, 2009.

643 Loza, C. L., Craven, J. S., Yee, L. D., Coggon, M. M., Schwantes, R. H., Shiraiwa, M., Zhang, X.,

644 Schilling, K. A., Ng, N. L., Canagaratna, M. R., Ziemann, P. J., Flagan, R. C., and Seinfeld, J. H.:

645 Secondary organic aerosol yields of 12-carbon alkanes, Atmospheric Chemistry and Physics, 14, 1423-

646 1439, 10.5194/acp-14-1423-2014, 2014.

647 Ma, P. K., Zhao, Y., Robinson, A. L., Worton, D. R., Goldstein, A. H., Ortega, A. M., Jimenez, J. L.,

648 Zotter, P., Prevot, A. S. H., Szidat, S., and Hayes, P. L.: Evaluating the impact of new observational

649 constraints on P-S/IVOC emissions, multi-generation oxidation, and chamber wall losses on SOA

650 modeling for Los Angeles, CA, Atmospheric Chemistry and Physics, 17, 9237-9259, 10.5194/acp-17-

651 9237-2017, 2017.

652 McDonald, B. C., de Gouw, J. A., Gilman, J. B., Jathar, S. H., Akherati, A., Cappa, C. D., Jimenez, J.

653 L., Lee-Taylor, J., Hayes, P. L., McKeen, S. A., Cui, Y. Y., Kim, S.-W., Gentner, D. R., Isaacman-

654 VanWertz, G., Goldstein, A. H., Harley, R. A., Frost, G. J., Roberts, J. M., Ryerson, T. B., and Trainer,

655 M.: Volatile chemical products emerging as largest petrochemical source of urban organic emissions,

656 Science, 359, 760-764, 10.1126/science.aaq0524, 2018.

657 Ng, N. L., Kroll, J. H., Chan, A. W. H., Chhabra, P. S., Flagan, R. C., and Seinfeld, J. H.: Secondary

658 organic aerosol formation from m-xylene, toluene, and benzene, Atmospheric Chemistry and Physics,

659 7, 3909-3922, DOI 10.5194/acp-7-3909-2007, 2007.

660 Pagonis, D., J. E. Krechmer, J. de Gouw, J. L. Jimenez and P. J. Ziemann: Effects of gas–wall

661 partitioning in Teflon tubing and instrumentation on time-resolved measurements of gas-phase organic

662 compounds. Atmos. Meas. Tech. 10(12): 4687-4696, 10.5194/amt-10-4687-2017, 2017.

663 Pandis, S. N., Paulson, S. E., Seinfeld, J. H., and Flagan, R. C.: Aerosol formation in the photooxidation

664 of isoprene and β-pinene, Atmospheric Environment. Part A. General Topics, 25, 997-1008,

665 https://doi.org/10.1016/0960-1686(91)90141-S, 1991.

666 Presto, A. A., Miracolo, M. A., Donahue, N. M., and Robinson, A. L.: Secondary organic aerosol

667 formation from high-NO(x) photo-oxidation of low volatility precursors: n-alkanes, Environ Sci

668 Technol, 44, 2029-2034, 10.1021/es903712r, 2010a.

669 Presto, A. A., Miracolo, M. A., Donahue, N. M., and Robinson, A. L.: Secondary Organic Aerosol

670 Formation from High-NOx Photo-Oxidation of Low Volatility Precursors: n-Alkanes, Environmental

671 Science & Technology, 44, 2029-2034, 10.1021/es903712r, 2010b.

672 Pye, H. O. T., and Pouliot, G. A.: Modeling the Role of Alkanes, Polycyclic Aromatic Hydrocarbons,

673 and Their Oligomers in Secondary Organic Aerosol Formation, Environmental Science & Technology,

674 46, 6041-6047, 10.1021/es300409w, 2012.

675 Roberts, J., Marchewka, M., Bertman, S., Goldan, P., Kuster, W., de Gouw, J., warneke, C., Williams,

676 E., Lerner, B., Murphy, P., Apel, E., and Fehsenfeld, F.: Analysis of the isoprene chemistry observed

677 during the New England Air Quality Study (NEAQS) 2002 Intensive Experiment, Journal of

678 Geophysical Research-Atmospheres, 111, D23S12, 10.1029/2006JD007570, 2006.

679 Robinson, A. L., Donahue, N. M., Shrivastava, M. K., Weitkamp, E. A., Sage, A. M., Grieshop, A. P.,

680 Lane, T. E., Pierce, J. R., and Pandis, S. N.: Rethinking organic aerosols: Semivolatile emissions and

681 photochemical aging, Science, 315, 1259-1262, 10.1126/science.1133061, 2007.

682   Sangiorgi, G., Ferrero, L., Perrone, M. G., Papa, E., and Bolzacchini, E.: Semivolatile PAH and n-

683   alkane gas/particle partitioning using the dual model: up-to-date coefficients and comparison with

684   experimental data, Environmental Science and Pollution Research, 21, 10163-10173, 10.1007/s11356-

685   014-2902-z, 2014.

686   Stark, H., Yatavelli, R. L. N., Thompson, S. L., Kimmel, J. R., Cubison, M. J., Chhabra, P. S.,

687   Canagaratna, M. R., Jayne, J. T., Worsnop, D. R., and Jimenez, J. L.: Methods to extract molecular and

688   bulk chemical information from series of complex mass spectra with limited mass resolution,

689   International Journal of Mass Spectrometry, 389, 26-38, https://doi.org/10.1016/j.ijms.2015.08.011,

690   2015.

691   Tajuelo, M., Rodriguez, D., Teresa Baeza-Romero, M., Diaz-de-Mera, Y., Aranda, A., and Rodriguez,

692   A.: Secondary organic aerosol formation from styrene photolysis and photooxidation with hydroxyl

693   radicals, Chemosphere, 231, 276-286, 10.1016/j.chemosphere.2019.05.136, 2019.

694   Takekawa, H., Minoura, H., and Yamazaki, S.: Temperature dependence of secondary organic aerosol

695   formation by photo-oxidation of hydrocarbons, Atmospheric Environment, 37, 3413-3424,

696   https://doi.org/10.1016/S1352-2310(03)00359-5, 2003.

697   Timonen, H., Cubison, M., Aurela, M., Brus, D., Lihavainen, H., Hillamo, R., Canagaratna, M., Nekat,

698   B., Weller, R., Worsnop, D., and Saarikoski, S.: Applications and limitations of constrained high-

699   resolution peak fitting on low resolving power mass spectra from the ToF-ACSM, Atmos. Meas. Tech.,

700   9, 3263-3281, 10.5194/amt-9-3263-2016, 2016.

701   Tkacik, D. S., Presto, A. A., Donahue, N. M., and Robinson, A. L.: Secondary Organic Aerosol

702   Formation from Intermediate-Volatility Organic Compounds: Cyclic, Linear, and Branched Alkanes,

703   Environmental Science & Technology, 46, 8773-8781, 10.1021/es301112c, 2012.

704   Worton, D. R., G. Isaacman, D. R. Gentner, T. R. Dallmann, A. W. H. Chan, C. Ruehl, T. W.

705   Kirchstetter, K. R. Wilson, R. A. Harley and A. H. Goldstein: Lubricating Oil Dominates Primary

706   Organic Aerosol Emissions from Motor Vehicles. Environmental Science & Technology, 48(7): 3698-

707   3706, 10.1021/es405375j, 2014.

708   Wu, C., Wang, C., Wang, S., Wang, W., Yuan, B., Qi, J., Wang, B., Wang, H., Wang, C., Song, W.,

709   Wang, X., Hu, W., Lou, S., Ye, C., Peng, Y., Wang, Z., Huangfu, Y., Xie, Y., Zhu, M., Zheng, J., Wang,

X., Jiang, B., Zhang, Z., and Shao, M.: Measurement Report: important contributions of oxygenated compounds to emissions and chemistry of VOCs in urban air, Atmos. Chem. Phys. Discuss., 2020, 1-37, 10.5194/acp-2020-152, 2020.

Wu, L., Wang, X., Lu, S., Shao, M., and Ling, Z.: Emission inventory of semi-volatile and intermediate-volatility organic compounds and their effects on secondary organic aerosol over the Pearl River Delta region, Atmospheric Chemistry and Physics, 19, 8141-8161, 10.5194/acp-19-8141-2019, 2019.

Xie, M., Hannigan, M. P., and Barsanti, K. C.: Gas/particle partitioning of n-alkanes, PAHs and oxygenated PAHs in urban Denver, Atmospheric Environment, 95, 355-362, https://doi.org/10.1016/j.atmosenv.2014.06.056, 2014.

Yang, W., Li, J., Wang, M., Sun, Y., and Wang, Z.: A Case Study of Investigating Secondary Organic Aerosol Formation Pathways in Beijing using an Observation-based SOA Box Model, Aerosol and Air Quality Research, 18, 1606-1616, 10.4209/aaqr.2017.10.0415, 2018.

Yuan, B., Chen, W. T., Shao, M., Wang, M., Lu, S. H., Wang, B., Liu, Y., Chang, C. C., and Wang, B. G.: Measurements of ambient hydrocarbons and carbonyls in the Pearl River Delta (PRD), China, Atmospheric Research, 116, 93-104, 10.1016/j.atmosres.2012.03.006, 2012.

Yuan, B., Hu, W. W., Shao, M., Wang, M., Chen, W. T., Lu, S. H., Zeng, L. M., and Hu, M.: VOC emissions, evolutions and contributions to SOA formation at a receptor site in eastern China, Atmospheric Chemistry and Physics, 13, 8815-8832, 10.5194/acp-13-8815-2013, 2013.

Yuan, B., Koss, A. R., Warneke, C., Coggon, M., Sekimoto, K., and de Gouw, J. A.: Proton-Transfer-Reaction Mass Spectrometry: Applications in Atmospheric Sciences, Chem Rev, 117, 13187-13229, 10.1021/acs.chemrev.7b00325, 2017a.

Yuan, B., Koss, A. R., Warneke, C., Coggon, M., Sekimoto, K., and de Gouw, J. A.: Proton-Transfer-Reaction Mass Spectrometry: Applications in Atmospheric Sciences, Chemical Reviews, 117, 13187-13229, 10.1021/acs.chemrev.7b00325, 2017b.

Zhao, Y., Kreisberg, N. M., Worton, D. R., Teng, A. P., Hering, S. V., and Goldstein, A. H.: Development of anIn SituThermal Desorption Gas Chromatography Instrument for Quantifying Atmospheric Semi-Volatile Organic Compounds, Aerosol Science and Technology, 47, 258-266, 10.1080/02786826.2012.747673, 2013.

738 Zhao, Y., Hennigan, C. J., May, A. A., Tkacik, D. S., de Gouw, J. A., Gilman, J. B., Kuster, W. C.,

739 Borbon, A., and Robinson, A. L.: Intermediate-Volatility Organic Compounds: A Large Source of

740 Secondary Organic Aerosol, Environmental Science & Technology, 48, 13743-13750,

741 10.1021/es5035188, 2014a.

742 Zhao, Y., Hennigan, C. J., May, A. A., Tkacik, D. S., de Gouw, J. A., Gilman, J. B., Kuster, W. C.,

743 Borbon, A., and Robinson, A. L.: Intermediate-volatility organic compounds: a large source of

744 secondary organic aerosol, Environ Sci Technol, 48, 13743-13750, 10.1021/es5035188, 2014b.

745 Zhao, Y., Nguyen, N. T., Presto, A. A., Hennigan, C. J., May, A. A., and Robinson, A. L.: Intermediate

746 Volatility Organic Compound Emissions from On-Road Diesel Vehicles: Chemical Composition,

747 Emission Factors, and Estimated Secondary Organic Aerosol Production, Environ Sci Technol, 49,

748 11516-11526, 10.1021/acs.est.5b02841, 2015.

749 Zhao, Y., Nguyen, N. T., Presto, A. A., Hennigan, C. J., May, A. A., and Robinson, A. L.: Intermediate

750 Volatility Organic Compound Emissions from On-Road Gasoline Vehicles and Small Off-Road

751 Gasoline Engines, Environ Sci Technol, 50, 4554-4563, 10.1021/acs.est.5b06247, 2016.

752 Zhu, J., Penner, J. E., Lin, G., Zhou, C., Xu, L., and Zhuang, B.: Mechanism of SOA formation

753 determines magnitude of radiative effects, Proceedings of the National Academy of Sciences of the

754 United States of America, 114, 12685-12690, 10.1073/pnas.1712273114, 2017.

755

756 **Table 1**. Fractions of product ions (m-1) ions in mass spectra, sensitivities and detection

757 limits of higher alkanes in NO^+ PTR-ToF-MS.

Compounds	Ions	Fractions of (m-1) ions (%)	Sensitivities (ncps/ppb)	Detection limit for 10 s integration (ppt)	Detection limit for 1 min integration (ppt)
n-Octane	$C_8H_{17}^+$	24	104.6	3.5	1.3
n-Nonane	$C_9H_{19}^+$	32	106.3	3.2	1.2
n- n-Decane	$C_{10}H_{21}^+$	39	120.9	3.5	1.3
n-Undecane	$C_{11}H_{23}^+$	44	140.9	3.3	1.2
n-Dodecane	$C_{12}H_{25}^+$	62	156.3	2.4	0.9
n-Tridecane	$C_{13}H_{27}^+$	61	186.6	2.1	0.8
n-Tetradecane	$C_{14}H_{29}^+$	64	220.7	1.9	0.7
n-Pentadecane	$C_{15}H_{31}^+$	84	205.5	1.7	0.6
n-Hexadecane	$C_{16}H_{33}^+$	95	/	1.6	0.6
n-Heptadecane	$C_{17}H_{35}^+$	82	/	1.8	0.7
n-Octadecane	$C_{18}H_{37}^+$	90	/	1.8	0.7
n-Nonadecane	$C_{19}H_{39}^+$	71	/	1.2	0.4
n-Eicosane	$C_{20}H_{41}^+$	86	/	1.9	0.7
n-Heneicosane	$C_{21}H_{43}^+$	/	/	2.0	0.7

758

759

Table 2. Mean concentrations of alkanes (C8-C21) in different sites worldwide.

Compounds	Formula	PRD, China[a] (ppt)	PRD, China[b] (ppt)	NCP, China[a] (ppt)	Paris, France[c] (ppt)	Pasadena, US[d] (ppt)
Octane	C_8H_{18}	482±488	50±49	412±270	/	/
Nonane	C_9H_{20}	208±186	43±32	252±162	14±13	/
Decane	$C_{10}H_{22}$	174±199	29±28	224±147	24±22	/
Undecane	$C_{11}H_{24}$	129±138	21±17	170±119	19±16	/
Dodecane	$C_{12}H_{26}$	122±120	/	129±86	22±21	8±1
Tridecane	$C_{13}H_{28}$	66±60	/	89±59	13±12	6±1
Tetradecane	$C_{14}H_{30}$	50±47	/	57±39	27±23	9±2
Pentadecane	$C_{15}H_{32}$	45±42	/	46±33	23±18	5±0.8
Hexadecane	$C_{16}H_{34}$	36±33	/	32±24	22±19	4±1
Heptadecane	$C_{17}H_{36}$	21±20	/	18±14	/	3±0.4
Octadecane	$C_{18}H_{38}$	13±14	/	11±9	/	1.6±0.5
Nonadecane	$C_{19}H_{40}$	5±9	/	4±7	/	0.7±0.2
Eicosane	$C_{20}H_{42}$	0.7±4	/	3±6	/	0.24±0.08
Heneicosane	$C_{21}H_{44}$	0.5±5	/	2±5	/	0.15±0.1

761   [a]: alkanes measured with NO+ PTR-ToF-MS; [b]: n-alkanes measured with GC-MS; [c]: n-alkanes from Ait-Helal

762   et al. (2014); [d]: n-alkanes from Zhao et al. (2014a).
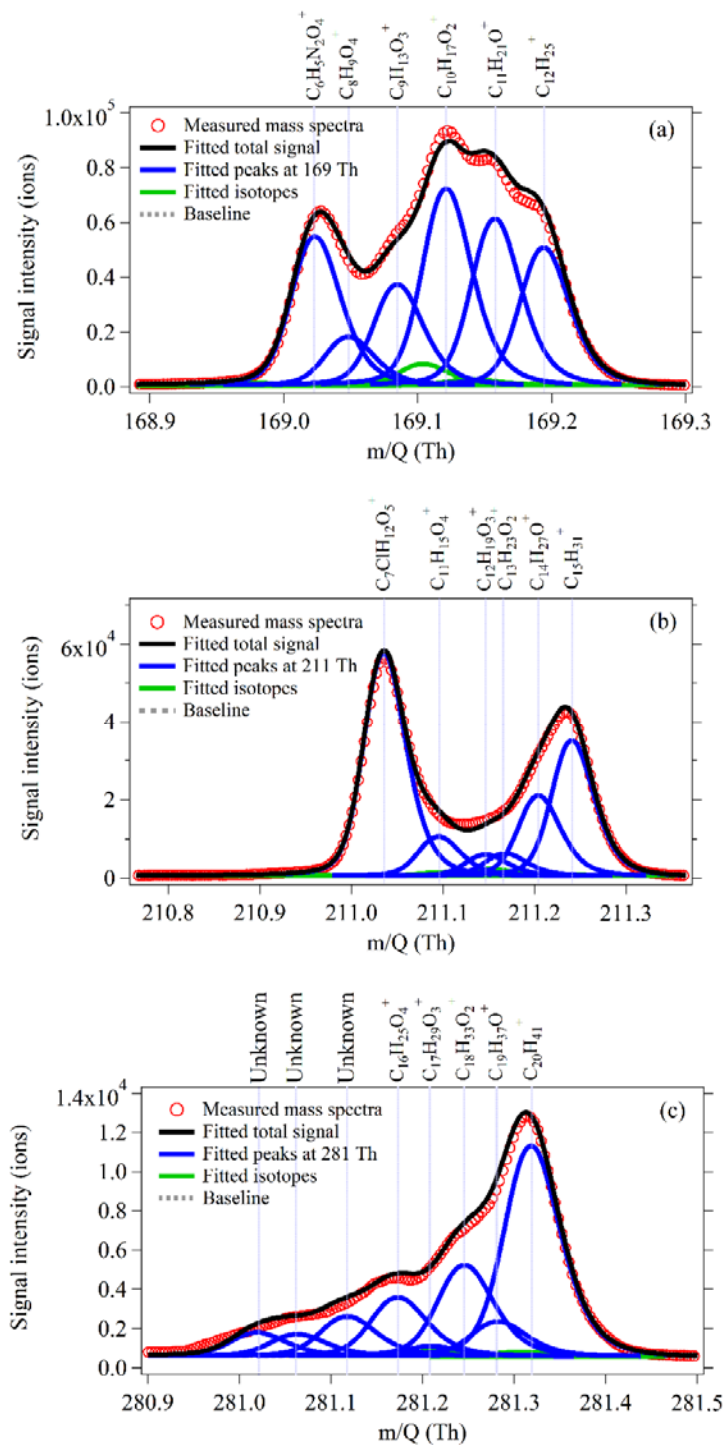
Figure 1. High-resolution (HR) peak-fitting to the averaged mass spectra on a typical day (12 October 2018) for m/z 169 **(a)**, m/z 211 **(b)** and m/z 281 **(c)**, at which masses produced by dodecane ($C_{12}H_{25}^+$), pentadecane ($C_{15}H_{31}^+$) and eicosane ($C_{20}H_{41}^+$) in NO^+ PTR-ToF-MS.

767
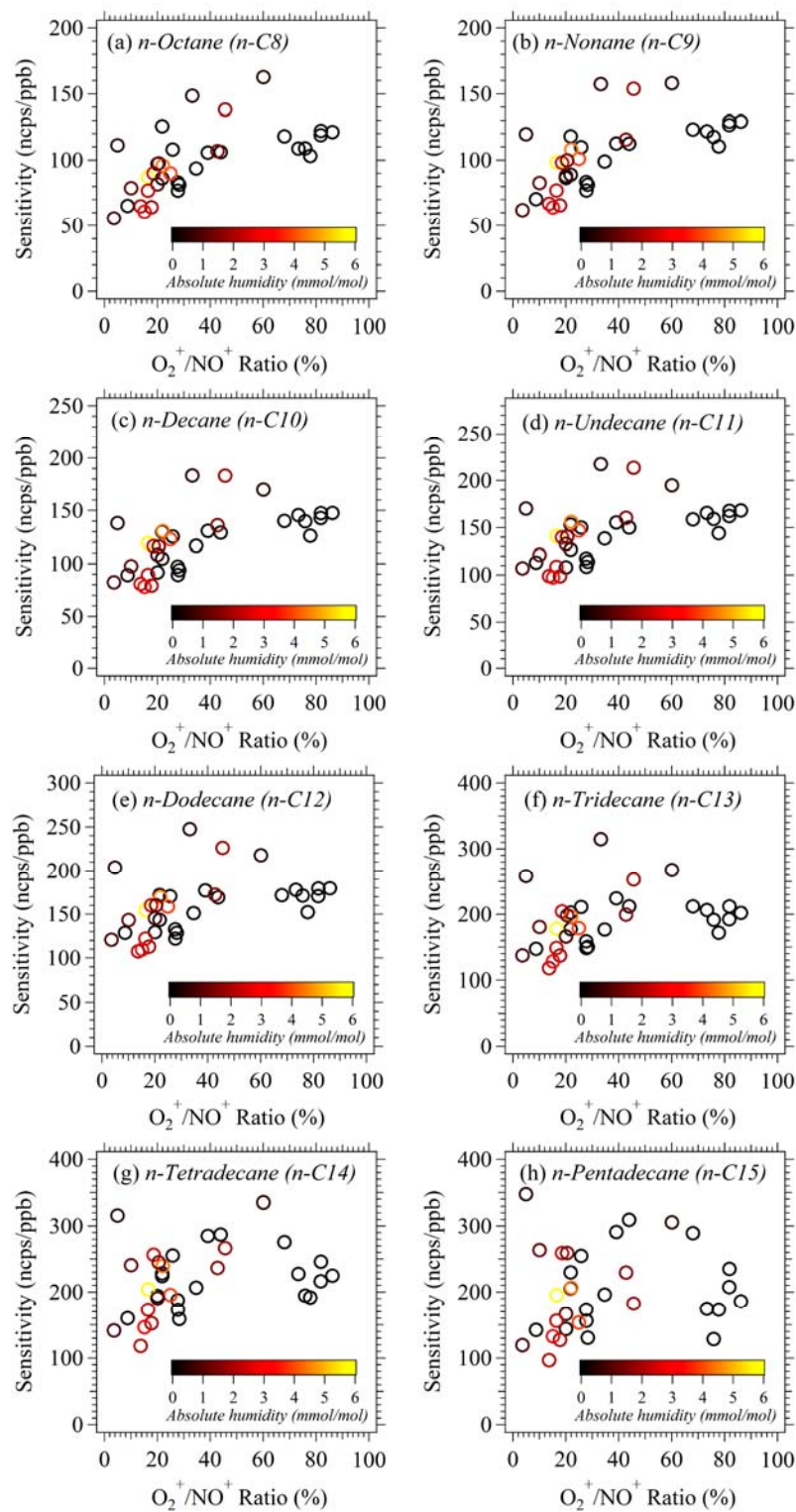
Figure 2. The relationship of sensitivities of *n*-alkanes (C8-C15) versus O_2^+/NO^+ ratios during

the NCP campaign. The data points are color-coded using absolute humidity during the

calibration.

771
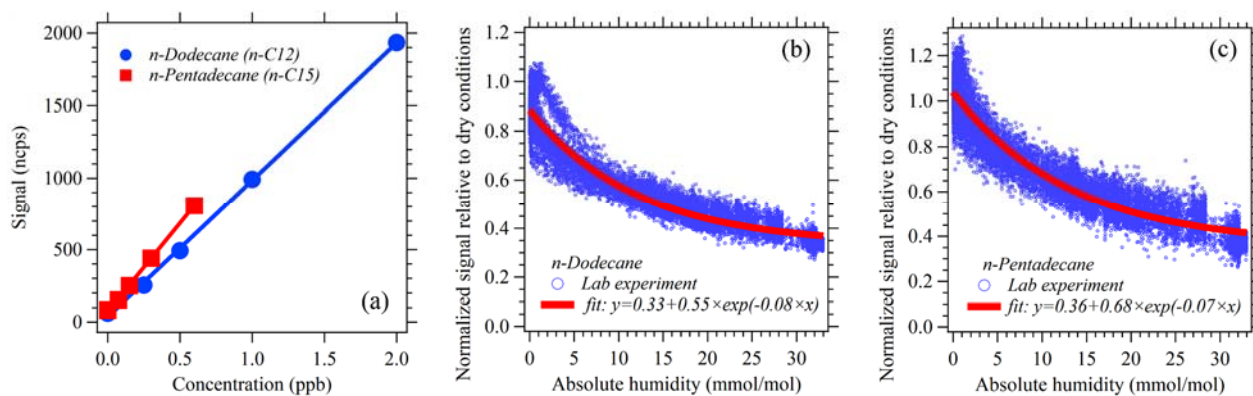
Figure 3. **(a)** Calibrations of *n*-Dodecane and *n*-Pentadecane under dry conditions; **(b)**

Humidity dependence of *n*-Dodecane. **(c)** Humidity dependence of *n*-Pentadecane.

774

775
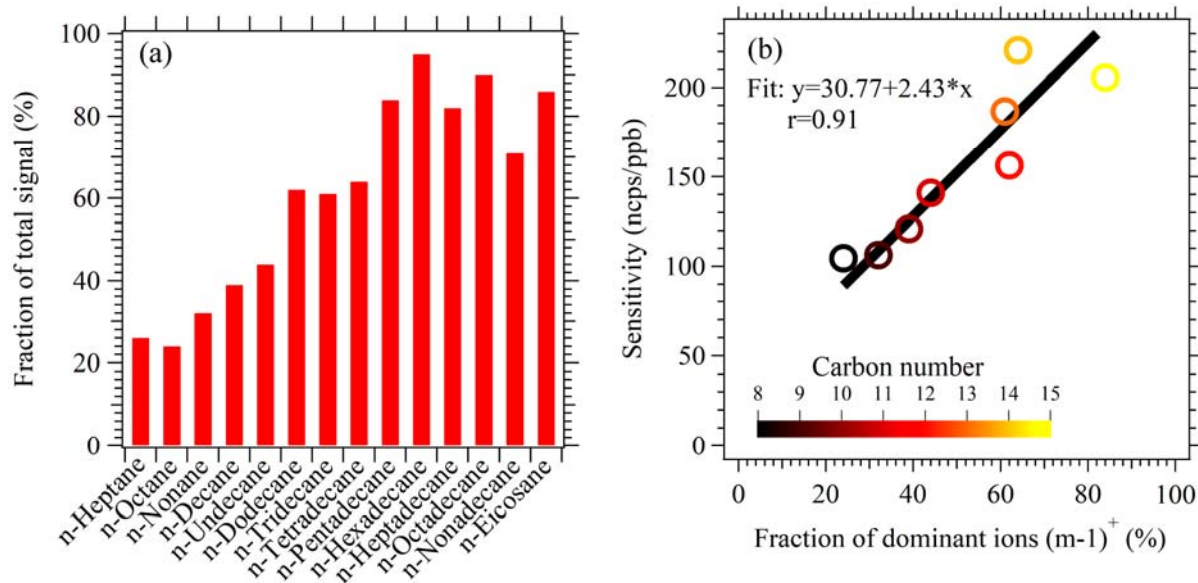
Figure 4. (a) The fractions of product ions (m-1) from hydride abstraction of C8-C20 *n*-alkanes

in NO+ PTR-ToF-MS. **(b)** Scatterplot of sensitivities under dry conditions versus the fractions

of hydride abstraction ions for C8-C15 *n*-alkanes.

779

780
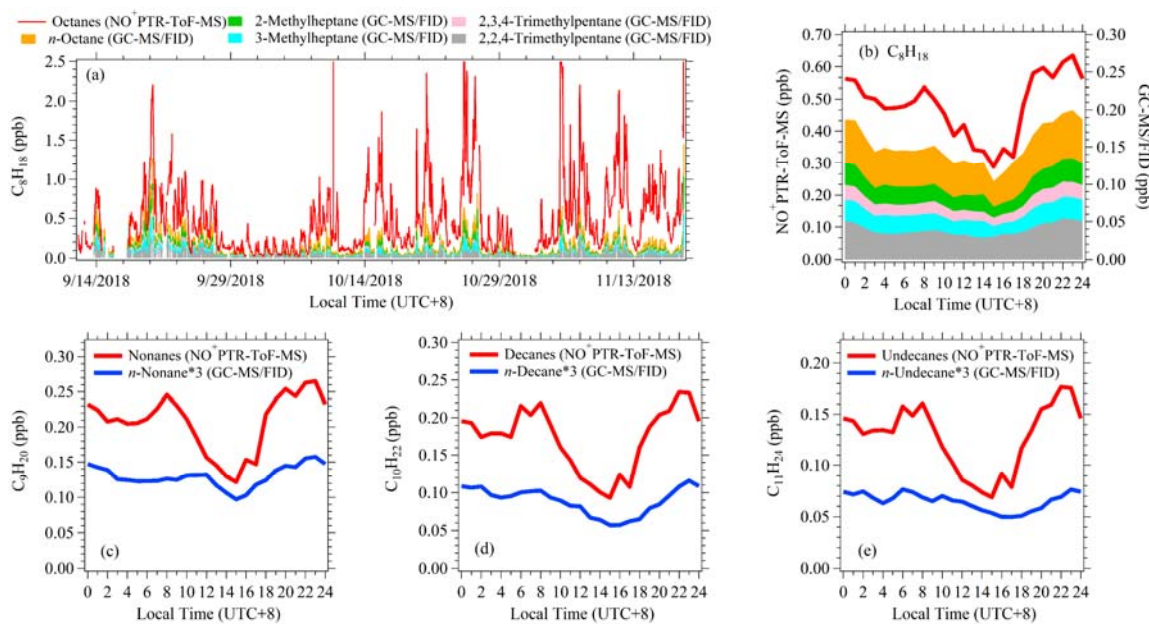
Figure 5. Comparisons of times series and diurnal variations of alkanes measured by NO^+ PTR-ToF-MS and GC-MS/FID in PRD. **(a)** Time series of C8 alkanes measured by NO^+ PTR-ToF-MS, C8 *n*-alkane and four branched isomers measured by GC-MS/FID. **(b)** Diurnal variations of C8 alkanes. **(c-e)** Diurnal variations of C9-C11 alkanes with NO^+ PTR-ToF-MS and C9-C11 *n*-alkanes with GC-MS/FID.
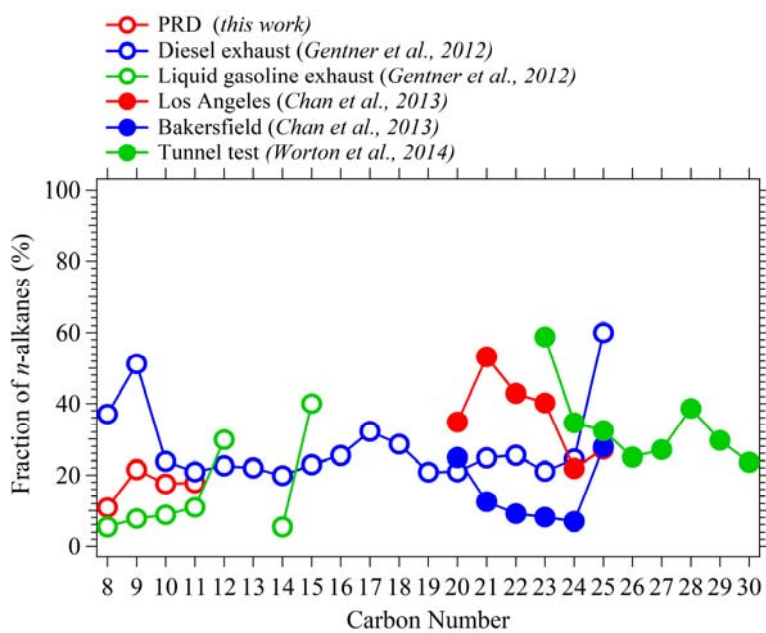
786

787 **Figure 6.** Fractions of *n*-alkanes in higher alkanes with same formulas in gas phase (hollow

788 dots) and particle phase (solid dots) derived from this study, ambient air in Los Angeles,

789 Bakersfield, Caldecott Tunnel and in vehicle exhausts (Chan et al., 2013; Gentner et al., 2012;

790 Worton et al., 2014).

791

792
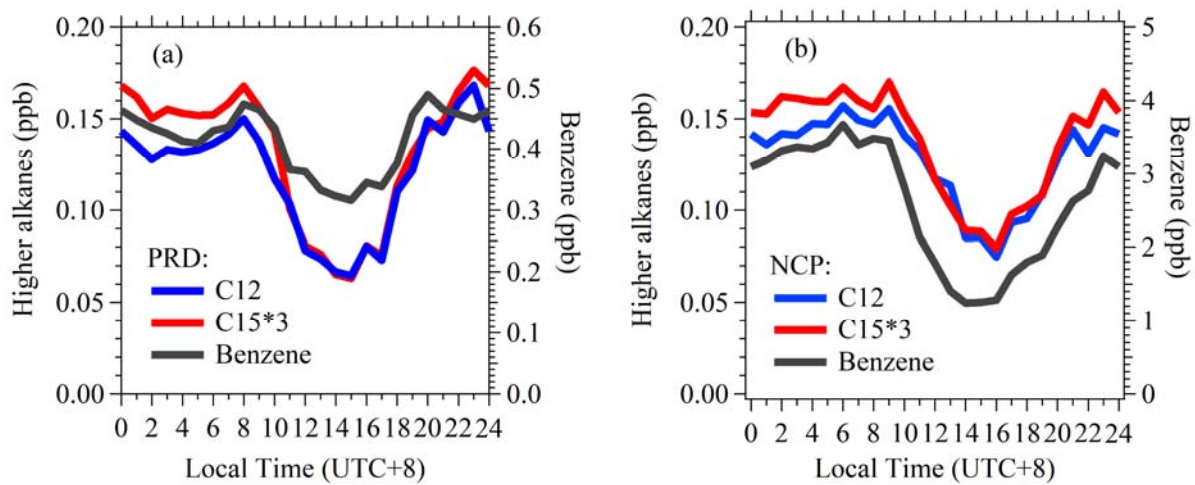
793

794 **Figure 7.** Diurnal variations of C12 alkanes, C15 alkanes and benzene in PRD **(a)** and NCP

795 **(b)**.

796
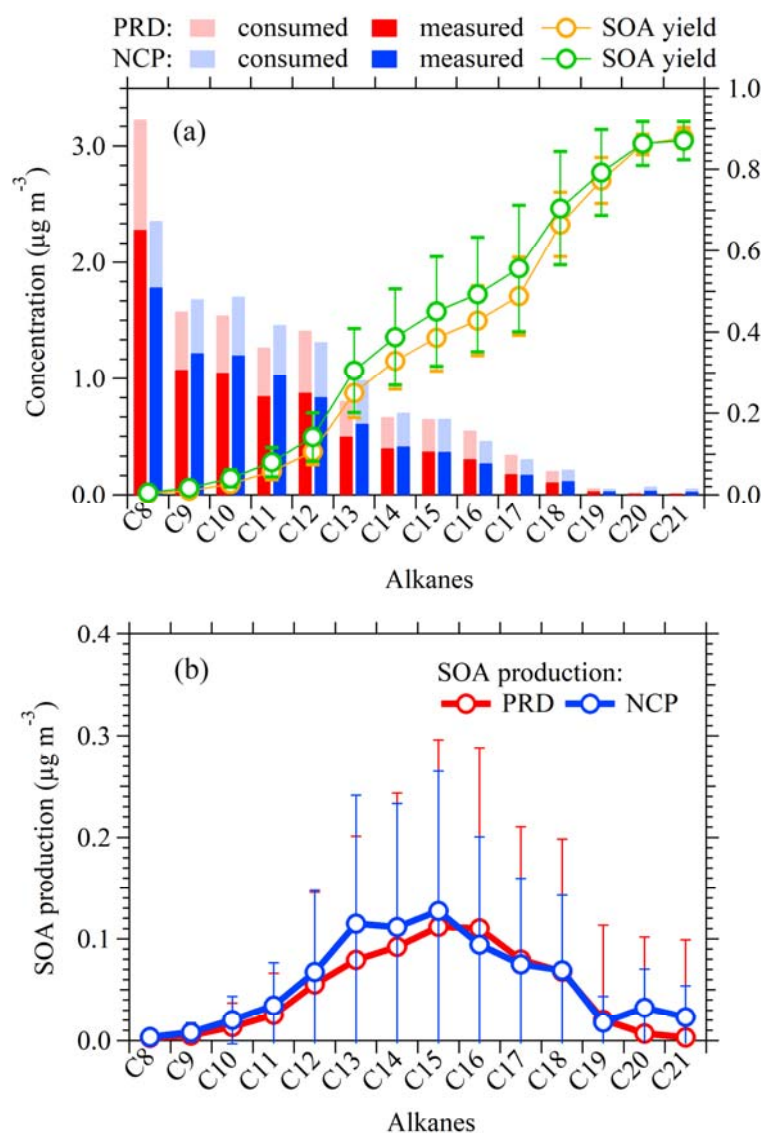
Figure 8. (a) Measured concentrations by NO⁺ PTR-ToF-MS, calculated consumed

concentrations and average SOA yields for C8-C21 alkanes in PRD and NCP. The consumed

concentrations represent the chemical losses of higher alkanes , which are calculated by using

the estimated SOA from each alkane dividing the corresponding SOA yields. The error bars

represent standard deviations (1δ) over the averaging period of calculated SOA yields. **(b)**

Calculated average SOA productions for C8-C21 alkanes in PRD and NCP. The error bars

represent standard deviations (1δ) over the averaging period of calculated SOA production.

804

805
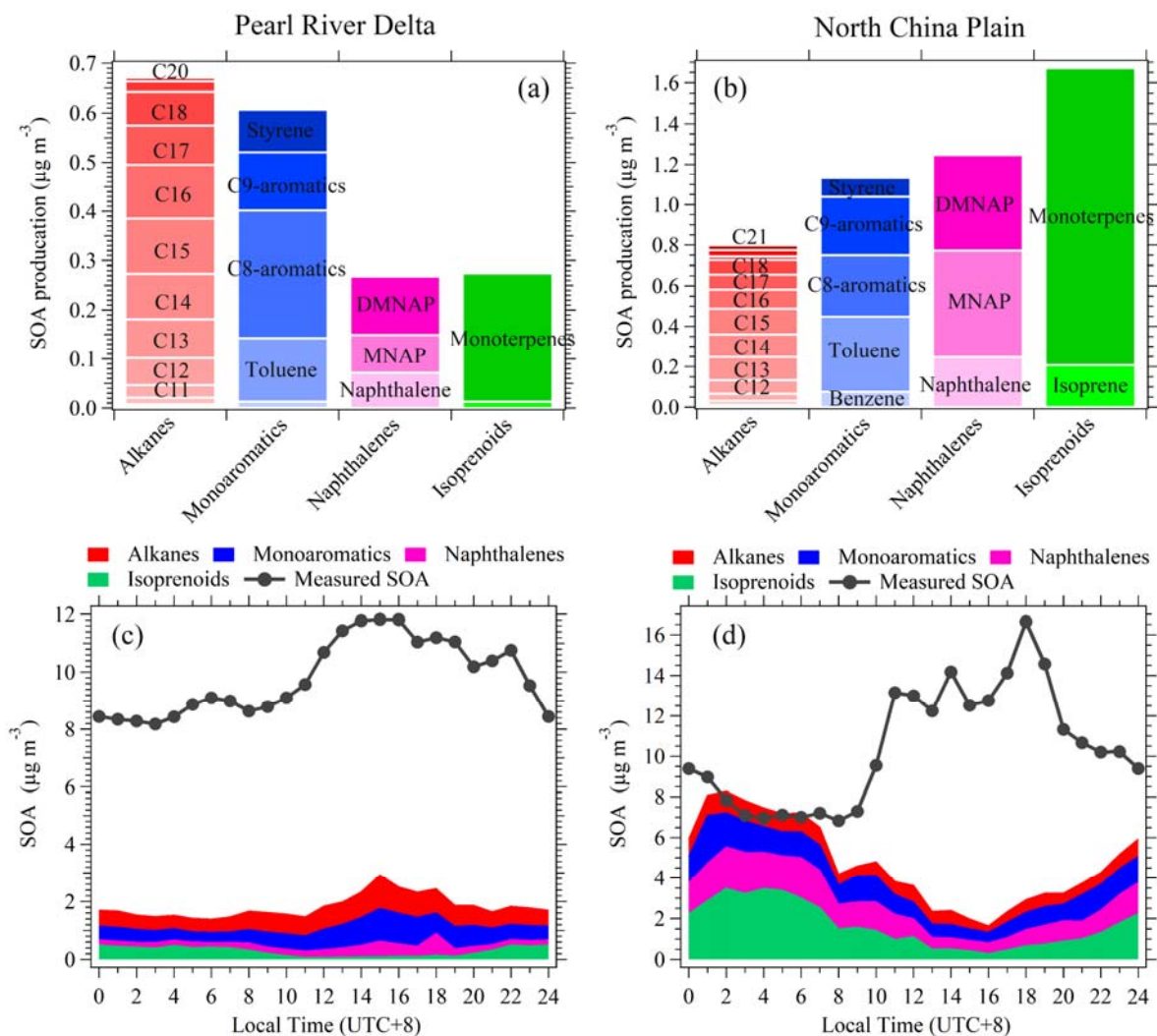
Figure 9. The mean concentrations of SOA produced from higher alkanes (C8-C21 alkanes), monoaromatics (benzene, toluene, C8 aromatics, C9 aromatics and styrene), naphthalenes (naphthalene, methylnaphthalenes, dimethylnaphthalenes) and isoprenoids (isoprene and monoterpenes) in PRD **(a)** and NCP **(b)**. Diurnal variations of SOA production from higher alkanes, monoaromatics, naphthalenes and isoprenoids as well as the measured SOA concentrations in PRD **(c)** and NCP **(d)**.